Lithium Ion Battery Aging Experiments at Sub-Zero Temperatures and Model Development for Capacity Fade Estimation

J. Jaguemont, L. Boulon, P. Venet, Y. Dubé and A. Sari.

***Abstract*— — Lithium-ion (Li-ion) batteries widely used in electric vehicles (EVs) and hybrid electric vehicles (HEVs) are insufficient for vehicle use after they have degraded to 70 to 80 percent of their original capacity. Battery lifespan is one of the largest considerations when designing battery packs for EVs/HEVs. Aging mechanisms, such as metal dissolution, growth of the passivated surface film layer on the electrodes, and loss of both recyclable lithium ions, affect the longevity of the lithium ion battery at high-temperature operations. Even vehicle maneuvers at low temperatures (T<0°C) contribute to battery lifetime degradation, owing to the anode electrode vulnerability to other degradation mechanisms like lithium plating. Nowadays, only few battery thermal managements have been properly considering with low-temperature degradation. This is due to the lack of studies on aging of Li-ion batteries at sub-zero temperature. This paper investigates how load cycle and calendar life properties affect the lifetime and aging processes of Li-ion cells at low temperatures. Accelerated aging tests were used to determine the effect of the ambient temperature on the performance of three 100Ah $LiFeMnP0_4$ lithium-ion cells. Two of them were aged through a normalized driving cycle at two temperature tests (-20°C and 25°C). The calendar test was carried out on one single battery at -20°C and mid-range of state-of-charge (SOC) (50%). Their capacities were continuously measured every two or three days. An aging model is developed and added to a preliminary single cell electro-thermal model to establish in future works a thermal strategy capable of predicting how the cell ages. This aging model was then validated by comparing its predictions with the aging data obtained from a cycling test at 0°C.**

***Index Terms*— Lithium-Ion; low temperatures; hybrid vehicles; aging mechanisms.**

I. Introduction

Over the past fifteen years, nearly every major automobile manufacturer in the world has been developing pure electric vehicles (EVs) and hybrid electric vehicles (HEVs) to counteract the rising oil prices and because of the increasing awareness of the environmental impacts of CO_2 emissions and local air pollution. EVs and HEVs have significantly reduced energy consumption and greenhouse gas emissions. With the growing popularity of electrified powertrains, the batteries used in these applications have become a common topic. Various fundamentally different battery technologies are currently being used from Nickel-Cadmium (NiCd) to Lead-Acid through Nickel-Metal hydride (NiMH) battery [1], [2]. However, this paper only focuses on the electrochemical energy storage using lithium-ion batteries because of their characteristics in terms of power-to-energy ratio [1], [3]. Currently, they appear to provide the most suitable performance characteristics for storing the electrical energy in EV or HEV applications.

Yet, cost [4], safety [5], charging times [6], recyclability [7], and charging infrastructure [8] are all common causes for concern. Perhaps most importantly, the batteries' reduced energy and power densities at low temperatures have been called into question. Experiences in cold climates with batteries in laptops, cell phones, and even HEV/EV batteries with large capacity size have caused this concern [9]–[11]. Poor performance of the battery at low temperature can be attributed to a rise of the internal impedance of the cell, which is present in every lithium-ion battery technology [11].

In places like Canada, Russia, or Scandinavian countries where the temperature during winter drops below -20°C that lasts for at least four to six months, driving an HEV/EV turns out to be a problem. Linked to this concern, one challenge is to understand the battery's electro-thermal behavior at this temperature level to develop a prime thermal strategy mandatory for use of an HEV/EV at sub-zero temperatures.

Many studies in the literature have discussed the effects of temperature on batteries [11]–[15]; they usually focus on presentations of battery tests under cold temperatures [11], [15]. In some instances, they are associated with a model establishment and validation for further battery thermal management [12]–[14]. In addition, among these studies, a previous work has been proposed [16] that reports an accurate electro-thermal model validated with tests on an actual HEV battery rated at 100Ah at very low temperatures (from -20° to 0°C), which is on target for an optimal battery thermal strategy.

Unfortunately, temperature is part of the aging process of the cell, which is not acknowledged in the current thermal strategies [17], [18]. The aging rate of batteries depends on a wide range of factors, and some of which are poorly

known. High temperature [19], current [20], and frequency [21] are among the possible factors, but the influence of sub-zero temperatures is much more misjudged. Loss of active material lithium [22] and solid electrolyte interface (SEI) growth [23] are found to be the main contributors to aging at high temperatures. At low temperatures, known aging process encompasses the lithium deposit as metal on the anode surface (so called lithium plating [24]) instead of lithium intercalation leading to a growth of the SEI, but currently there is a lack of data on aging at low temperatures.

The objectives of this paper are to present an aging study of lithium-ion cells at sub-zero temperatures and to develop an aging model built on [16] to predict the remaining capacity of an HEV Li-ion battery in a cold environment as the cell ages for a future thermal strategy development.

To realize this model, accelerated aging tests were carried out on three HEV batteries. Two were cycled at 25°C and -20°C under a normalized driving profile. One was stored at a very low temperature and mid-charge (50% SOC) to determine the effect of the storage temperature on cells. Data collected from the experimental tests were used to determine the coefficients of the models that are based on mathematical equations. Simulation results from the aging model were compared with a cycle aging test done at 0°C to validate the aging model.

The rest of this paper is organized as follows: Section II presents the experimental setup for the aging tests and the results associated with it. Section III describes the aging model. Section IV discusses the results of simulations compared to experimental tests carried out to validate the aging model. Finally, conclusions are given in Section V.

II. Experimental setup

This section presents the experimental setup for the characterization and validation of the aging model.

A. Battery feature

Four rectangular $LiFeMnP0_4$ batteries were tested to accomplish the aging test procedure. The cells have a nominal capacity of 100 Ah and a voltage range of 2.5–3.8V. Even though this study is looking toward an HEV application, the cells were tested individually to simply understand the degradation caused by cold temperatures. In future studies, the cell arrangement could consist of a battery pack.

B. Aging test

Battery aging tests can be categorized into cycle aging test and calendar aging test. Both tests were carried out by

the same experimental test bench schematized in Fig. 1. An Arbin BT-2000 battery cycler was employed for cycling, calendar aging (in this case, the current is zero), and capacity measurement. A computer with an Arbin software interface controls all the cycling stations and treats the data acquired from the test bench, including the current, I_{batt}, the cell voltage, V_{cell}, and temperature. On that note, limited acquisition input slots on the Arbin station allowed using a thermocouple to monitor the cell temperature. As shown in Fig. 2, it was placed on the electrode (negative), T_{core}, because it rejects more heat than the surface under current solicitations [9], [25]–[27], thus it is the best place to observe the temperature variations of the cell core.

To recreate the cold environment climate, a climatic chamber was used; it is independent from the rest of the bench and is self-controlled to maintain the aging temperature test called, T_{test}, that is, the temperature of the chamber. The tested cell was placed in the chamber for calendar, cycling, or capacity measurement. The data collection took place in the AMPERE laboratory located in Lyon, FRANCE. The aging lab contained a number of battery aging stations, which were all carefully monitored.

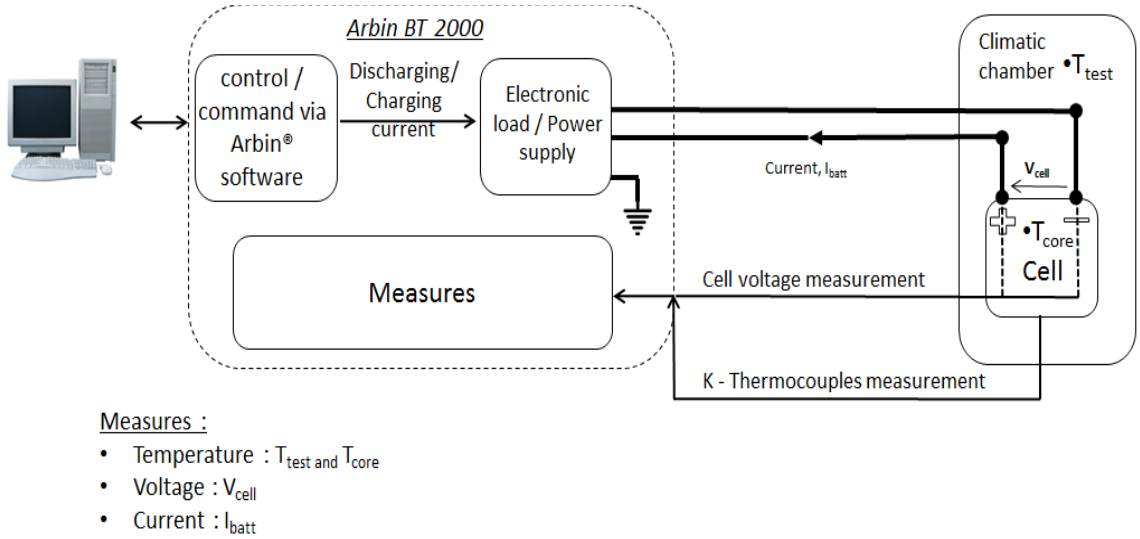

Fig. 1. Experimental test bench.

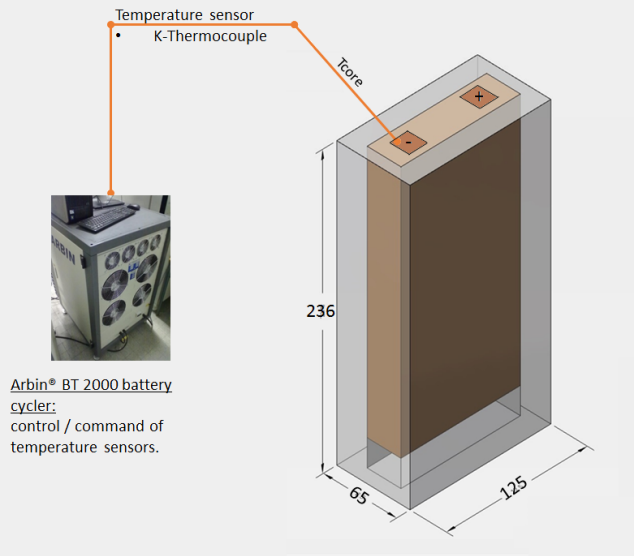

Fig. 2. Display of the K-type thermocouple for temperature data acquisition.

1) Calendar aging test

Calendar aging occurs while the cell is in storage. In other terms, it is the irreversible cell's loss of capacity when the battery is not used [14], [23]. The test procedure for an accelerated calendar test is simple; the cell is charged to a predefined SOC and stored at the requested temperature of storage with no floating voltage. Lack of testing material compelled us to experiment on one cell, thus only one temperature and one state-of-charge (SOC) were tested. The cell was exposed to a cold temperature of -20°C corresponding to an average temperature during winter in Canada. As for the value of the SOC, a mid-charge state (50%) was chosen to minimize the outcome of the SOC impact on the cell [28], and this allowed us a better observation of the temperature effect. The fully charged cell was discharged at 1C rate (100A) to the desired SOC. The cell temperature was then allowed to drop to the target cold temperature for 8h to reach the thermal equilibrium, and the cell voltage was left to drift.

2) Cycle aging test

Cycle aging occurs when the cell is either charging or discharging. The current solicitations, the temperature conditions, and the operation mode of the battery are factors in the cycle aging. The cycling test procedure focuses on finding the correlation between driving conditions in a real application and the fundamental aging processes in the battery cell. Two cells underwent a driving cycle presented in Fig. 3 until they have degraded to 70 to 80 percent of their original capacity. The cycle aging test exposed the two cells to two temperatures (25°C and -20°C), one SOC (60%), and one ΔSOC (20%), where ΔSOC is the window of nominal capacity of the cell discharged during the cycle. Here it should be underlined that other aging factors like depth-of-discharge (DOD) [29] and discharge rates [30] are

out of the scope of this paper.

The driving profile (Fig. 3a) was conceived for an urban EV driving application. It is composed of 3 phases: discharging, resting, and charging. Each phase lasts one hour and succeeds each other alternatively to reach a 5-hour driving profile. The current profile for the discharging phase was taken from an Electric Toyota Prius running a standardized cycle known as the New European Driving Cycle (NEDC) (see Fig. 3b). The details of the sequences are explained as follows:

- Sequence 1: in this driving profile, the cell starts at 60% charge state to avoid exceeding the upper or lower voltage limits with high current rates that accelerate the lifetime of the cell; an SOC of 50% appeared to be sufficient enough to prevent these damages. The cell at a 60% charge state is discharged for 1h to a 50% SOC corresponding to a driving sequence of an EV user from home to workplace. The discharge profile is actually a micro-discharging cycle of 800s extended to 3600s (see Fig. 3b).

- Sequence 2: the cell is kept resting for one hour. At first, the time of rest was agreed to be a resting phase during a working day of 7–8 hours. However, to execute multiple cycles per day, the time was shortened to 1h corresponding to the necessary time for T_{core} to reach thermal equilibrium with the chamber, T_{test}. Moreover, compared to cycle aging, calendar lifetime has few impacts on cell degradations, thus seven hours can be stripped of the resting sequence without harming the cell too much. Additionally, the calendar aging results presented in section E.2 emphasizes this point. This is also a reason why a mid-charge SOC was performed in the calendar aging tests.

- Sequence 3: the cell is going through a discharging phase (see sequence 1) again but to a lower SOC (40%) matching the return trip of the EV driver.

- Sequence 4: the cell is charged up to an SOC of 60% with a constant current of 0.25C. This sequence compensates the capacity spent in sequences 1 and 3, which is analogous to the EV user's recharging procedure of the EV at home.

- Sequence 5: the cell is kept at rest for 1h corresponding, for instance, to a non-utilization of the EV. Same explanations as for sequence 2 apply for this sequence.

The cycling at -20°C started after 8h of rest at each temperature for the cell interior, T_{core}, to reach the thermal equilibrium with the temperature of the chamber, T_{test}.

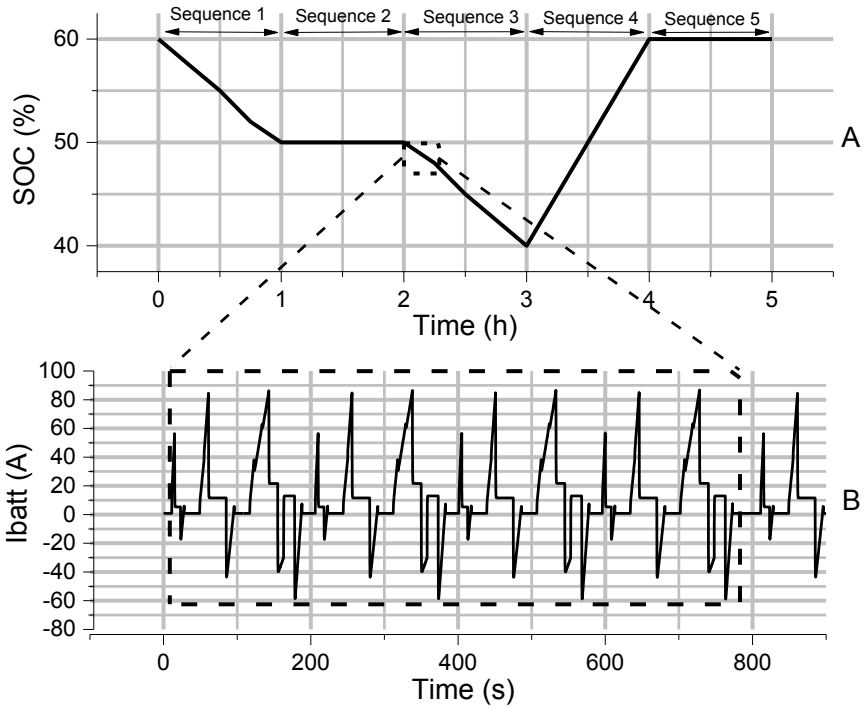

Fig. 3. (a) Schematic of the driving profile used for the cycle aging test. (b) The first 800 seconds of the standardized NEDC cycle.

C. Capacity measurement

The capacity measurement test is designed to acquire as much information as possible about the cell regularly during a life test of a cell. This test monitors the progression of the battery aging by extracting the cell capacity as it degrades. Capacity measurement tests were performed every two or three days at the aging temperature (T_{test}) using a few test cycles only. They consisted of standard capacity tests, constant current (CC), constant voltage (CV) charge, and CC discharge tests. Each test cycle started with a charging regime at 1C rate (100A) to 3.8V and held at 3.8V until the current dropped to a current of 0.05C (5A). Subsequently, the cell was rested and then discharged at 1C rate to a cut-off voltage of 2.5V. The rest period between charging and discharging was 30 min at 25°C and 45 min at -20°C for the cell to come close to a thermal equilibrium state with T_{test}. After another resting time, the cell was charged following the same CC-CV protocol. Finally, the cell was discharged to the desired SOC – 50% or 60% for calendar aging test and cycle aging test, respectively.

D. Resistance increment assessment

In addition to the remaining capacity extraction, cell resistance was evaluated during each capacity measurement test using: [31]

$$R_p = \frac{V_1 - V_0}{I_{batt}} \quad (1)$$

where R_p is the discharge pulse resistance (Ω), V_1-V_0 is the voltage difference (V) caused by the current pulse, and I_{batt} is the current passing through the cell (A). In this study, a 2s pulse resistance was considered.

E. Aging test results

This subsection presents the cell aging test results of the cycle and calendar experiments from two points of view: the capacity fade and the resistance increment. All test results for the three different aging tests are reported in Tables I and II.

1) Cycle aging test results

Fig. 4 shows the results measured in the cycle test at both temperatures. The gradual discharge curves of the capacity measurement test vs discharging time are displayed for the two temperature tests of 25°C (Fig. 4a) and -20°C (Fig. 4b).

First, from the comparison of the two experimental graphics (Fig. 4a and Fig. 4b), one can observe the impact of the test temperature on the cell electrical performances. At -20°C (Fig. 4b), a strong voltage drop is seen at the beginning of the trial. The literature [1] attributes this drop to the Nernst's equation [1], [32] and explains the dependence of the cell voltage to the temperature as follows:

$$E = E_0 - \frac{RT}{nF} ln \frac{a(ox)}{a(red)} \quad (2)$$

where a_i is the activity of the relevant species (ox for oxidizers and red for reducers), R is the gas constant (J/mole/K), T is the temperature (K), E is the cell voltage (V), and E_0 is the standard potential (V). After 250s, the voltage curve experiences an important voltage rise potentially due to the electrochemical processes inside the cell and the electron density passing through the circuit leading to a significant heat generation from the cell. According to [9], [33], heat generation rates are produced by various sources, but only joule heating (ohmic) prevails at this current rate over the other resistances. It follows a voltage benefit attributed to the lower cell impedance due to a higher temperature of the cell [34].

In most cases, ideal conditions are usually specified by the manufacturer, such as 25°C, a voltage range, etc. These conditions are intended to represent the anticipated decreasing operating performances of the battery during aging. However, as shown in Table I, the end of life criterion (80% of the nominal capacity) of the 100Ah lithium-ion cell given by the manufacturer was found to be extremely inaccurate with the results. At ambient temperature (25°C), 7% of the capacity is lost after 170 cycles, which is by extension very dissimilar to the results reported by the manufacturer (2000 cycles).

As a rule, when the cell ages, its capacity decreases (fades), and its internal resistance increases. It is thought that the cells at higher temperatures botched before the ones at lower temperatures [35], [36]. As surprising as it is, the conventional limit of 20% capacity loss referring to the nominal capacity 80 Ah at -20°C is reached only after a dozen cycles, which is equivalent to 60h. The main cause of this large capacity loss is that at subzero temperature, the reactions between the lithium ions entering the anode and the electrolyte (Li intercalation) induce another aging mechanism [23], [24]. After a literature survey, there are some known aging phenomena [24], [36]:

1) Loss of cyclable lithium [24] due to massive consumption for the formation.

2) Growth of the passivation layer around the anode known as the solid electrolyte interphase (SEI) [37].

3) Growth of the SEI layer during aging is also engendered by the cathode main metal (Mn, Fe, or Co) dissolution.

4) Consequence of 3) is the transition from the cathode of the metal and then its deposition on the anode [24], [37].

5) Minor effect of 3) is the loss of positive active material that also counts for capacity fades [36]. All these mechanisms are accelerated at high temperature [38].

Logically, when the cell is down to below 0°C, the phenomena quoted above should be slowed or not prevalent. However, as shown in Fig.4b, the aging rate of the cell is still accelerated at low temperature. In [39], the authors explained the occurrence of this increasing lithium loss rate at sub-zero temperature with another aging mechanism: the lithium plating. By measurements with pouch cells with the reference electrode, the authors showed a negative polarization with respect to Li/Li^+ in the low temperature range. This polarization far surpasses the lithium plating potential (100mV)[40], which signifies a high possibility of metallic lithium deposition at lowered temperatures. Post-mortem studies of the pouch cells revealed that the anodes were indeed plated with grey metallic lithium. This lithium plating leads to capacity loss by interfering with the Li intercalation between the anode and electrolyte and a loss of lithium (electrolyte decomposition) [39], which dramatically affects the cell lifetime.

As for the cell internal impedance, Fig. 5a shows the evolution of the cell resistance through the aging cycles. A focus on this plot (Fig. 5a) displays an increase of the cell resistance as the cell ages. This is mainly caused by reduced electrolyte conductivity due to the consumption of salt during the formation of the SEI and aging [37]. Another way to demonstrate its increment is to plot the thermal evolution of cell during each capacity measurement test. Figs. 5b and 5c display the temperature of the cell, T_{core}, vs the capacity of the cell for each cycle number for the two T_{tests}.

First, comparing between Figs 5b and 5c shows that low temperature operation significantly increases the impedance of the cell. The ΔT, which is the difference of the temperatures between the final temperature and the initial temperature for a given cycle number, is 14°C at -20°C, whereas at 25°C, ΔT= 12°C. The reasons for the rise of the impedance are reduced conductivity of the electrolyte and decreased diffusivity of the Li^+ inside the cells due to the SEI growth [20], [38].

Moreover, for the lower temperature (Fig. 5c), this effect is stronger. This is due to the aging phenomenon, the lithium plating, which is consuming the negative electrode area. The net consequence of the latter is an increase of the charge-transfer resistance at the electrolyte-anode interface [36], [40], [41].

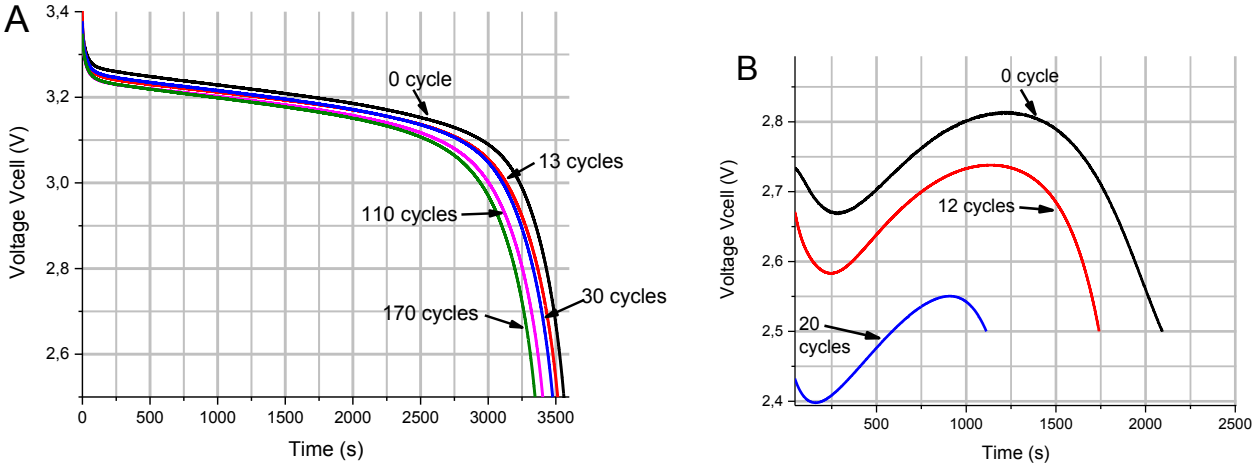

Fig. 4. (a) Capacity measurement test for cycle aging at 25°C. (b) Capacity measurement test for cycle aging at -20°C.

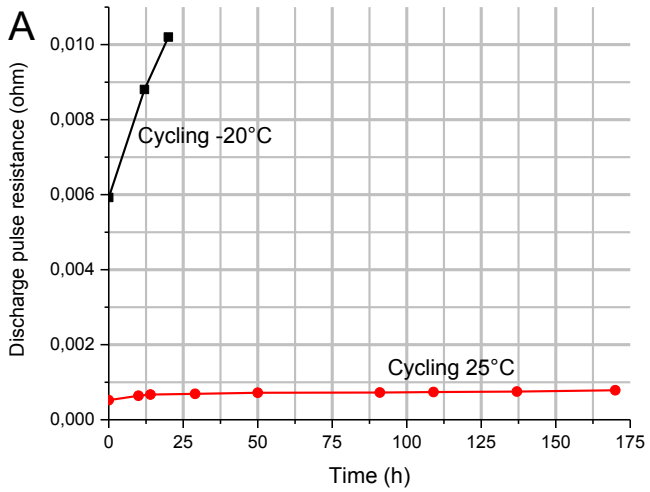

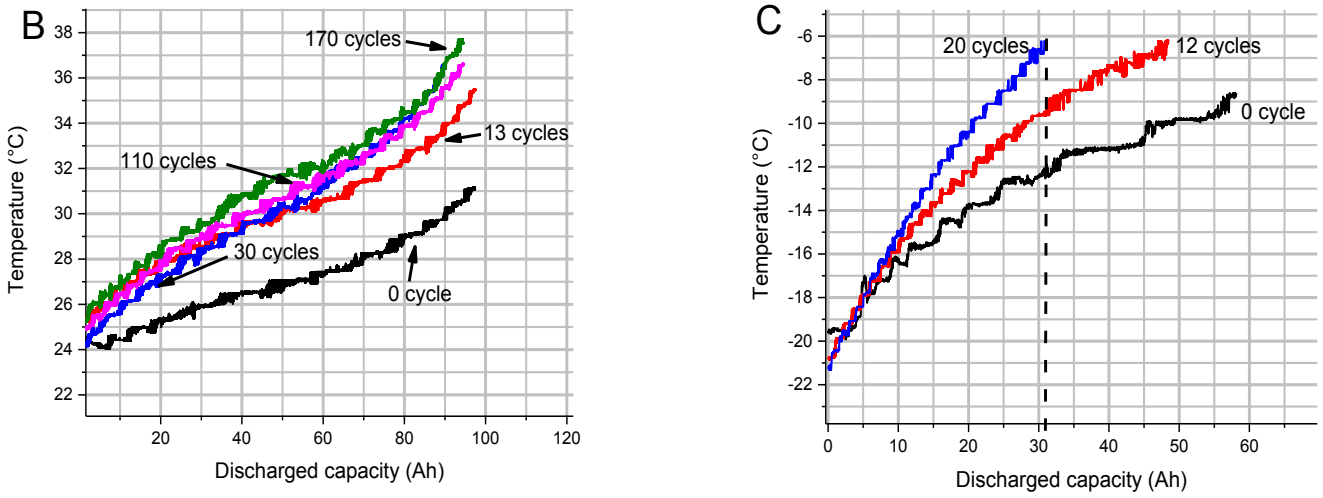

Fig. 5. (a) Evolution of the resistance for both cycle aging test (25°C/-20°C) (b) Evolution of the temperature T_{core} vs discharging capacity for cycle aging test at 25°C. (c) Evolution of the temperature T_{core} vs discharging capacity for cycle aging test at -20°C

2) Calendar aging test results

Figure 6 shows the results of the calendar capacity loss test at -20°C. The end of the life criterion (80% of the nominal capacity) is reached in less than 415h of storage time, which corresponds to 17 days. As expected, for the same temperature T_{test}, a lower capacity fade than cycle aging is seen, as calendar aging is caused by the battery storage time (e.g., self-discharge, impedance rise [36]). Hence, aging effects occurring within the battery like loss of cyclable lithium or active material may be slowed, but they are still a major concern.

For the resistance increment assessment shown in Fig. 7a, the same conclusion as for the cycle aging test is made. As shown in Fig. 7a, the progressive rise of the impedance during aging is significant due to the same but less impacting

aging mechanisms as cycling. Fig. 7b, which represents the evolution of the cell temperature with calendar aging, emphasizes this point. Nevertheless, this increase has a negative impact on the battery performances as explained above.

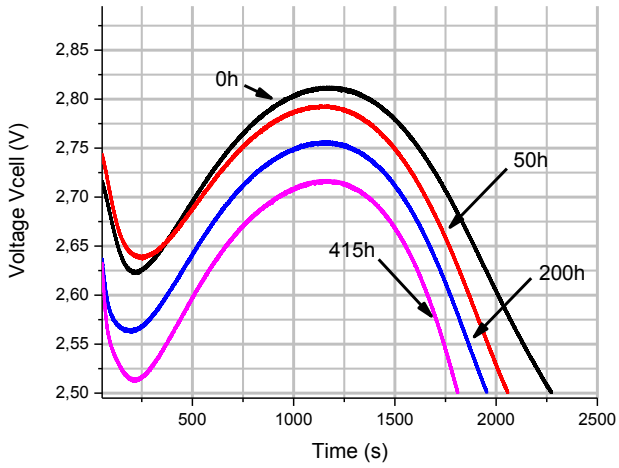

Fig. 6. Capacity measurement test for calendar life at -20°C.

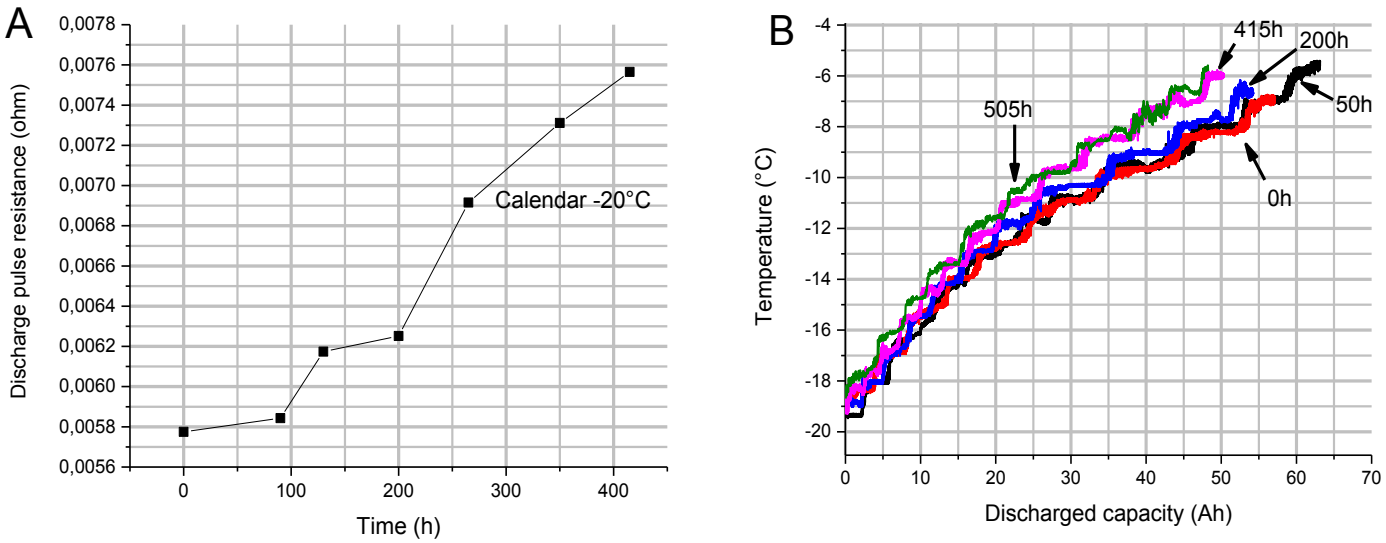

Fig. 7. (a) Evolution of the resistance increment with calendar aging at -20°C. (b) Evolution of the temperature T_{core} vs discharging capacity for calendar life test at -20°C.

3) Calendar / cycling effect

The data from the calendar aging test at -20°C allowed us to quantify the effects (%) of the calendar and cycling, at the same temperature, on the cell. An estimation of the effects of each aging process can be done on the driving cycle

at -20°C. The effects were reported in Table I and calculated as follows:

At -20°C, the degradation for calendar aging is 20.3% in 415 hours that corresponds to, 4.89e-2% of loss of lithium/hour. In the driving profile, 2 hours are dedicated to calendar aging, so in one cycle, 9.8e-2% of lithium is lost due to calendar aging at -20°C.

In a cycle,

$$\%calendar_{loss} = 2 \times 4.9e^{-2} = 9.8e^{-2}(\%\ of\ lithium\ loss/cycle) \quad (3)$$

Thereby, in 12 cycles (the EOL), 1.17% is lost due to calendar aging. In the end, in the driving cycle at -20°C, 20.8% is lost after 12 cycles. Therefore, calendar aging accounts for 5.6% of these losses.

$$\%calendar_{effect} = \frac{12 \times \%calendar_{loss}}{Total\ \%lithium\ loss\ in\ 12\ cycles} = \frac{1.17}{20.8} = 5.6\% \quad (4)$$

Moreover, at 25°C, the quantification of the two aging processes is 50%/50%, as in this study, the impact of cycling aging on the cell degradation is considered as harmful as the calendar aging at this temperature. A literature survey emphasizes this point. In [42], at ambient temperature (30°C), the degradation rate and internal resistance increment for cycle aging and calendar aging are close: 0.03% versus 0.05% after 32 days. The results in Table I show that at low temperature, cycle aging has much more greater effect than calendar aging.

4) Aging results conclusion

As a result, low temperatures show a strong connection with cell aging. Ensuring an accurate prediction of the cell capacity fade and resistance increment as the cell ages in cold weather is critically important to build a thermal strategy for HEVs/VEs. Therefore, a thorough battery model that can determine the remaining capacity of the battery with aging through a range of temperatures is important.

TABLE I. OUTPUT EXPERIMENTAL DATA OF THE CAPACITY MEASUREMENT TEST

T_{test} (°C)	Test characteristics				
	Testing	***Initial capacity measured (Ah)***	***Final capacity measured (Ah)***	***Number of cycle (or time) before end-of-life criterion (80% of the cell initial capacity)***	***Calendar effect / Cycle effect (%)***
25	Cycling	99.8	92.9	*170 cycles = 850 hours (7% of capacity loss) (from a 60% SOC to a 0% SOC)*	*50% / 50%*
-20	Cycling	58.6	46.4	*12 cycles = 60 hours (from a 60% SOC to a 40% SOC)*	*5.6% / 94.4%*
-20	Calendar	63.1	50.3	*415(hours) at 50% charged*	*100% / 0%*
25	Manufacturer' s data curve	100	80	*2000 cycles = 20000 hours (from a 100% SOC to a 0% SOC at 0.1C (10A).*	

TABLE II. OUTPUT EXPERIMENTAL DATA OF THE RESISTANCE INCREMENT CALCULATION

T_{test} (°C)	Test characteristics				
	Testing	***Number of cycle (or time): instant measure.***	***Measured resistance (mΩ)***	***T_{core} initial value (°C)***	***T_{core} maximal value (°C)***
25°C	Cycling	*0 cycle*	0.52	24.2	31.1
		170 cycles = 850 hours	0.78	24.6	37.3
-20°C	Cycling	*0 cycle*	5.92	-19.6	-8.6
		12 cycles = 60 hours	8.88	-20.8	-6.19
-20°C	Calendar	*0 (hours)*	5.77	-19.4	-6.90
		415 (hours)	7.56	-18.7	-5.91

III. AGING MODEL DEVELOPMENT

This section discusses the modeling of batteries and puts the accent on modeling of the degradation processes present in the batteries. First, a brief discussion on the art of battery models is required.

A. State-of-art

Cell aging is a complex mechanism. There are two main observable variations in a cell as it ages: a loss of capacity and a rise of its impedance. To evaluate those aging indicators, many methods have been documented in the literature. They are divided into three parts: electrochemical models[43], performance-based models [44], [45], and equivalent

circuit-based models. Here, the objective is to obtain a representation of the battery's aging behavior that has a good balance among accuracy, tuning simplicity, and simulation duration. Consequently, a semi-empirical model is designed (electric circuit-based).

An equivalent circuit model representation encompasses an ideal voltage source, an internal resistance, and "n" parallel RC circuits, where n is the order of the model. All the aforementioned parameters are considered variant during the battery aging process [46].

Additionally, an electro-thermal model built on the equivalent circuit model methodology has been proposed [16], exploring the variation of the cell performance loss during cold weather operation. The purpose of this model is to develop a battery thermal management system for severe winter applications. The model uses a MATLAB/Simulink® interface, and it is based on the Thevenin model [47]. It has been validated on experimental data taken from an actual HEV Li-Ion battery (rated at 100Ah). Multiple discharging tests were executed at different low temperatures, namely, -20°C, -10°C, and 0°C. Parameters were identified using the experimental data, and the resulting model provided suitable voltage and temperature responses.

Nonetheless, this model does not consider all the changes in the battery capacity and battery impedance caused by battery degradation occurring in cold climates. Therefore, this paper focuses on the development of a lifetime model from this simple model [16] to account for the variation of capacity loss rate and the resistance increment during cycle aging and storage at low temperature to pursue an optimal battery thermal strategy.

B. General aging model

In this study, two principal effects of battery aging are identified: capacity fade and resistance increment. Both differ on their consequences, thus having different chemical sources.

1) The effect of capacity fading

The chosen battery model [16] is an equivalent circuit model. As it is defined as simple, it is perfectly suitable for optimization because it can be easily integrated in a battery management system (BMS) [48]. This model represents, in a suitable way, the dynamic behavior of the battery, to which the effects of the temperature have been added. A representation of the simplified model is displayed in Fig. 8. The battery output voltage of the Li-ion cell is calculated due to the battery open circuit voltage (OCV), voltage drop resulting from the battery ohmic resistance (R_0), and battery polarization impedance (R_1C_1 circuit). It is represented by the following formula [49]:

$$V_{cell} = OCV - R_1 I_1 - R_0 I_{batt} \quad (5)$$

where I_1 is the polarization current expressed as [46]:

$$\frac{dI_1}{dt} = \frac{(I_{batt} - I_1)}{R_1 C_1} \quad (6)$$

Below is a description of the role the open-circuit voltage (OCV). It represents the difference of the electrical potential between the two electrodes of the cell when the cell is in open-circuit connection. In [16] and [44], the authors have shown that this voltage is only strongly dependent upon the SOC and very little on the temperature:

$$OCV = f(SOC) \quad (7)$$

where SOC is the state-of-charge of the cell and is expressed as

$$SOC = SOC_0 - \int \frac{I_{batt}}{C_{init}}\, dt \quad (8)$$

where C_{init} is the initial capacity measured of the cell in Ah and SOC_0 is the initial state-of-charge of the cell.

However, the internal impedance block composed of one RC circuit and an ohmic resistance, takes into account both the varying state of charge, and the rise of the cell temperature, which transforms (5) into the following:

$$V_{cell} = OCV(SOC) - R_1(SOC,T) I_1 - R_0(SOC,T) I_{batt} \quad (9)$$

As mentioned earlier, the effect of capacity fading must be considered in modeling the capacity thermal and electrical behaviors for a battery. The capacity fading is the translation of the loss of usable capacity of a battery due to storage time, temperature, and cycle number. The loss occurs when the battery is inoperative (calendar life losses [24]) or employed (cycle life losses [20]).

Thus, the irreversible loss causing capacity fading leads to a capacity correction factor (CCF) to assess the remaining usable battery capacity. It is stated as:

$$CCF = 1 - k_1(T,N) - k_2(T,t) \quad (10)$$

where, k_1 is the aging factor caused by cycle life. It is a function of the cycle number (N) and the temperature (°C). k_2 is the aging factor caused by calendar aging. It is temperature- (°C) and time- (h) dependent.

Then, the available capacity, C_{av}, of the battery is defined as a function of the CCF, which is expressed as:

$$C_{av} = C_{init} \times CCF \quad (11)$$

And this transforms equation (8) into:

$$SOC = SOC_0 - \int \frac{I_{batt}}{C_{av}}\, dt \qquad (12)$$

As a result, the model includes a factor that represents the capacity degradation of the battery obtained as a consequence of cycling, storage, and temperature tests.

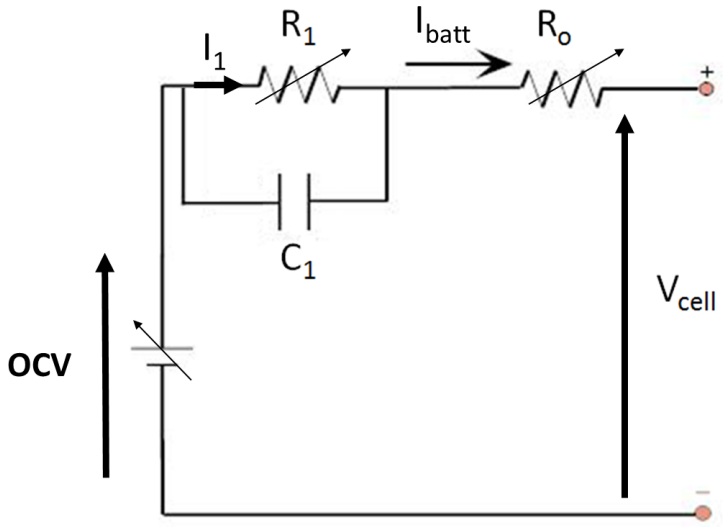

Fig. 8. Schematic of the Thevenin model

2) The effect of resistance increment

The internal impedance block consists of a series resistor composed of an ohmic resistance and one RC network. All are temperature- and SOC-dependent. However, the internal impedance also experiences an increment as a result of cycle and calendar aging. Thereby, the equivalent impedance is divided into three terms, as follows:

$$Z_{increment} = Z_{eq}.k_3(N,T).k_4(T,t) \qquad (13)$$

And in accordance with [50]:

$$Z_{eq} = \frac{R_1}{1+sR_1C_1} + R_0 \qquad (14)$$

where k_3 is the cycling factor accountable for the increment of the impedance, expressed as a function of the cycle number and the temperature (°C), and k_4 is the calendar aging factor, which is time- and temperature-dependent.

As discussed in Section II.E, the resistance increment is seen during the gradual cell temperature through both calendar and cycle aging. Therefore, the following estimation of the resistance increment is a continuation of the thermal model presented in [16]. The thermal model is centered on the next equations [50], and it is illustrated in Fig.

9:

$$dU/dt = Q_{gen}\,(t) - Q_{loss}\,(t) \qquad (15)$$

where U, the internal energy, is the total energy contained by a thermodynamic system, here the core, expressed in Joules. The following assumptions are made for the thermal model:

1. Due to the moving liquid electrolyte inside the core, the temperature of the core, T_{core} (the temperature of the inner cell), is assumed to be uniform. In this paper, uniformity of T_{core} happened to be sufficient for thermal simulation.

2. For uniformity of T_{core}, a linear temperature gradient settles between T_{core} and the temperature of the crust; T_{crust} (the temperature of the surface of the cell) (see Fig. 9).

3. For simplification, current distribution and heat generation in core are assumed to be uniform during the operation process. It is difficult to acquire the thermal conductivities of battery in x, y, and z directions, so this paper assumes that the heat conductivity inside the lithium core is uniform and invariant with the operating status.

4. The thermal capacity of the crust of the cell is assumed as negligible against the thermal capacity of the core.

5. In this paper, heat generation is characterized only by ohmic losses because of their simplicity to model, contrary to other losses where an electro-chemical usually simulates them [20]. Then, based on these assumptions:

$$Q_{gen} = R_0.(I_{batt})^2 + R_1.(I_1)^2 = R_{eq}.(I_{batt})^2 \qquad (16)$$

Q_{gen} is the generating heating rate (W), or the rate of the heat generation occurring in the cell core.

Finally,

$$Q_{loss} = Q_{cond} = Q_{conv} \qquad (17)$$

with Q_{cond} (W) as the conductive heat transfer and Q_{conv} (W) the convective heat transfer. The conductive heat transfer between the core and the crust can be calculated as:

$$Q_{cond} = \frac{(T_{co} - T_{cr})}{R_c} \qquad (18)$$

where T_{core} and T_{crust} represent the temperature at the core and the crust of the cell, respectively. R_c is the thermal conductivity resistance associated with the conductive heat flux. The heat transfer from the crust to the surrounding is estimated and determined by:

$$Q_{conv} = h_{conv} S_{area} (T_{crust} - T_{air}) \qquad (19)$$

Hence, Q_{conv} depends on the air flow temperature, T_{air}, the area of heat exchange, S_{area}, and the convective heat transfer coefficient $h_{conv.}$ The physical parameters can be found in the literature or with an experimental exploration. In this paper, the first option is chosen, and Table III shows all the parameters needed to operate the model.

TABLE III
BATTERY PHYSICAL PARAMETERS

Symbol	QUANTITY	Value
C_p	Specific heat capacity ($J.g^{-1}°K^{-1}$).	3.58[1]
λ	Thermal conductivity of air ($W.m^{-1}.°K^{-1}$)	0.02620 at 20°C[50]
h_{cond}	Conductive heat transfer coefficient ($W.m^{-2}.°K^{-1}$)	0.30 at 20°C[50]
h_{conv}	Convective heat transfer coefficient ($W.m^{-2}.°K^{-1}$)	5 (natural convection)[50]
m	Battery mass (kg),	2.1 (manufacturer)

As the internal impedance increases through aging, the increment estimated by (13) obtained from pulse discharge resistance (1) is directly counted into (16).

As a consequence, the degradation model will now account for both capacity fade and resistance increment at the same time. But in order to obtain a reliable lifetime prediction of the cell under different cycling test, storage times and temperature conditions, a clear separation of these aging effects is needed.

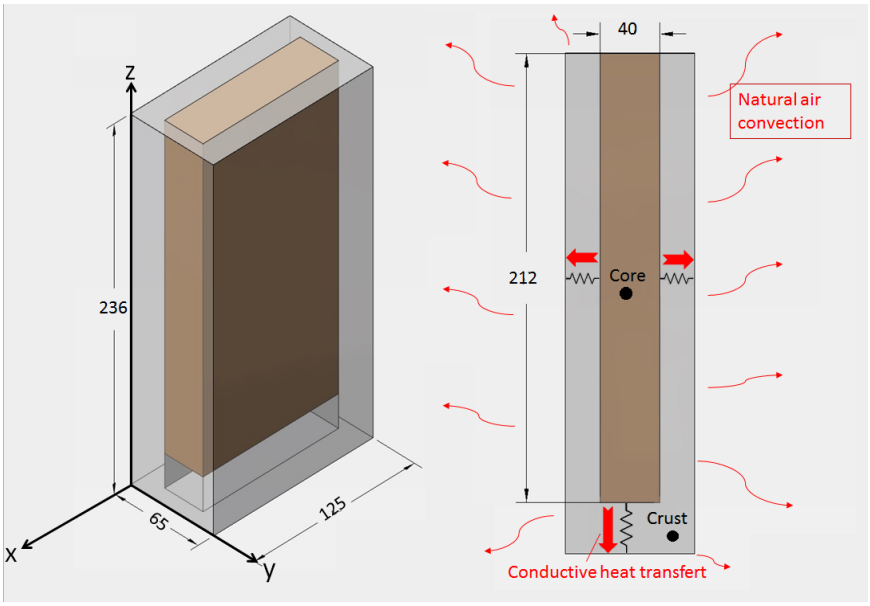

Fig. 9. Schematic of the battery thermal model.

C. Calendar aging

Calendar aging refers to a loss of capacity during storage time. The main variables for modeling are time and temperature; this paper considers a range of use of the battery around a point of the SOC and, therefore, neglects the SOC effect on aging [48].

1) Arrhenius' law

In general, it is a common practice to fit the calendar aging result with Arrhenius' law [44], [51]. It appears that the aging rate has an Arrhenius-like kinetic.

$$v = A.exp^{(\frac{-E_a}{RT})} \quad (20)$$

where v is the aging rate, A is the pre-exponential factor, E_a (KJ/mol) is the activation barrier, R is the gas constant (J/mol/K), and T is the temperature of aging (K).

This law is used in many studies that consider storage temperatures [46], [52], [53]. In [44], the authors exhibit in 2003 that capacity fades during calendar aging follow an Arrhenius law. Also, in [52], the authors determine the activation barrier, E_a, of Li-ion cells for calendar aging with Arrhenius law. In [53], the impact of aging on the state-of-energy is depicted and reproduced via the Arrhenius theory.

However, the Arrhenius-like behavior used in these studies is only valid in certain temperature intervals that do not cover temperatures that EV/HEV might be exposed to during winter operations (-20°C to 0°C). At subzero temperature, the aging rate does not follow the Arrhenius law because of the presence of another mechanism: the lithium plating [39]. Therefore, for this model development, an alternative is sought instead.

2) Mathematical modeling.

In [54], Broussely et al. proposed a model that accounts for the capacity loss rate during accelerated calendar aging at high temperature. From this simple model, the corrosion rate was found to be time-dependent as $t^{1/2}$. Since then, numerous studies have been following this linear law [51], [54]. [51], [55]. However, there is a lack of aging model at low temperatures; thereby, we first adapted this mathematical for cold weather applications.

Nonetheless, this mathematical law simple model doesn't fit well with the experimental results. Thereby, a regression with a 4th polynomial order is chosen. The fitting equation is then:

$$\%_{loss}(T,t) = k_2 = a.t + b.t^2 + c.t^3 + d.t^4 \quad (21)$$

with a = 0.2, b = -7.6e-4, c = 1.1e-6, and d = -1.8e-10.

To verify the accuracy of the calendar aging model, an error calculation was performed for five points corresponding to five storage times. The error between the simulated value and the experimental data were calculated by:

$$\varepsilon_{k2} = \frac{|Li_{exp} - Li_{sim}|}{0.2Li_{exp}} \times 100 \quad (22)$$

where ε_{k2} is the error on the parameter k_2 (%), Li_{exp} is the capacity loss experimental value due to calendar aging capacity (%) and Li_{sim} is the capacity loss simulation value (Ah) at a given time. The error is actually the error based on the useful lifetime of the cell: 0-20% (a 0.2 coefficient a t the denominator). In addition, the maximum value was determined as follow:

$$\varepsilon_{k2max} = \max(\varepsilon_{k2}) \quad (23)$$

with ε_{k2} is the maximum error of the data points (%).The results of the error calculation are displayed in table IV. The maximum value was 1.6% for a storage time of 16h. This error calculation shows that the original fitting at -20°C gives similar results to the simulation, thus proving the good performance of the calendar aging model.

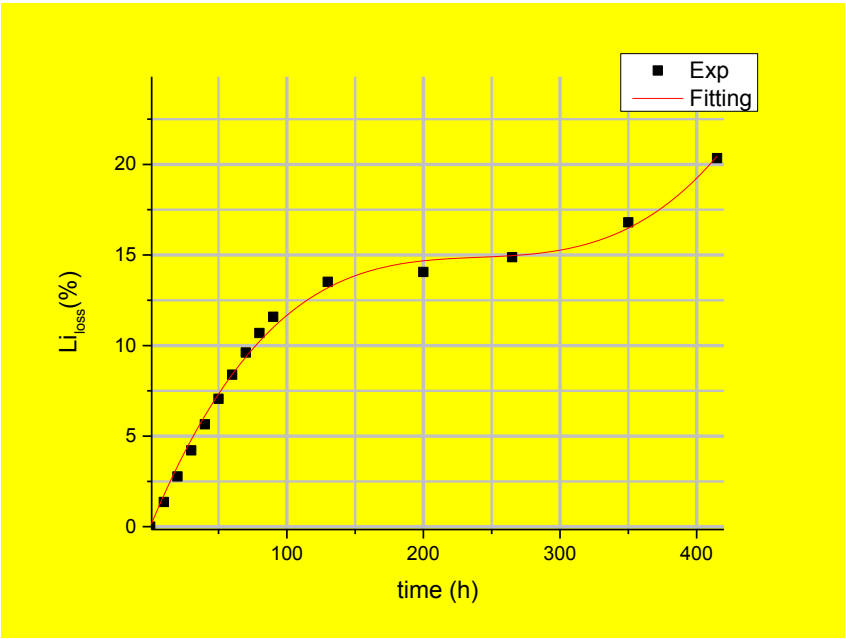

Fig. 10. Lithium loss vs storage time at -20°C for both experimental and simulation data with a polynomial fitting.

TABLE IV. ERROR CALCULATION OF THE CALENDAR AGING MODEL

Ttest (°C)	*Observation*	*Storage time (h)*	*Measured value*	*Simulated value*	*Error (%)*
-20°C	Lithium Loss (%)	*15*	1.3%	1.32%	1.6
		75	9.8%	10%	2
		200	14.7%	14.9%	1.4
		350	17.1%	16.9%	1.45
		415	20.3%	20.1%	1

D. Cycle aging

There are already some researches on the aging models of lithium-ion batteries cycle life [20], [45], [56]–[58]. Ploehn et al. [56] defined the loss of cyclable lithium proportional to the thickness of the SEI layer and the activation barrier. Additionally, Wang et al. [20] developed a complex capacity loss model considering the influence of the charge and discharge rate, depth of discharge, and working temperature modeled by the Arrhenius' law (20). As also discussed in the previous subsection, this latter methodology is not valid for our application because the area of the law of Arrhenius validity does not include low temperatures (<0°C) [39].

Yet, other aging models presented in the literature [45], [56], [57] evoked a typical cycle number dependency model for cycle aging. They addressed the thickness of the SEI layer as linear or simple function to the cycle number. Thus, in this study, the model for cycle aging is developed according to their investigations. Therefore, the capacity loss during cycle aging can be expressed as:

$$k_1(N) = \%_{loss}(N) = \beta.N \qquad (24)$$

where β is the coefficient of proportionality, and N is the cycle number.

Considering this equation (24) for each temperature of aging, T_{test}, the degradation level obtained now follows dependence like the cycle number and temperature of aging. For a better graphic understanding, a two-dimensional graph was realized with MATLAB®'s curve-fitting tool, representing the capacity fade (i.e. k_1) with a color graph as a function of cycle number and temperature. The 2Ds is presented in Fig. 11, where a sudden rise in lithium loss can be observed at low temperatures. Then, curve fitting was done using MATLAB's curve-fitting tool. The type of fit employed was a custom equation:

$$k_1(N) = a + b.\sin(m.T.N.\Omega) + c.exp^{-(w.N)^2} \qquad (25)$$

with a = 60.46, b= -3.6, c = -41.6, m = 0.19, and w = 0.089 as the fitting parameters, and N and T are the variables accounting for the cycle number and the temperature, respectively. It has to be underlined that the limits of the model (range of validity) are represented in the dark zone in Fig. 11 where the End-of-Life criterion is over 20%.

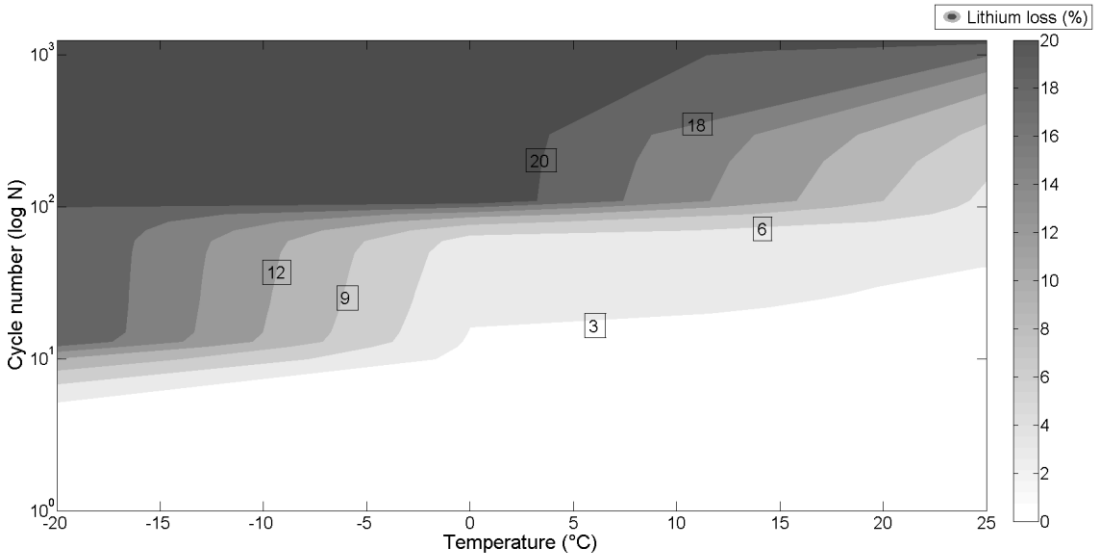

Fig. 11. 2D plot of k_1 as a function of cycle number and temperature, in case of aging produced by cycling.

E. Resistance increment

As already described in section II.D, the cell impedance was taken at each capacity measurement test during the discharging phase. The voltage dropped immediately after the current was applied. This pulse step in voltage helps in calculating the internal resistance at progressive aging states, based on equation (1).

Similarly to cycle aging modeling, previous works [57], [58] reported that the resistance increment is a function of the storage time, temperature, and cycle number. They observed that the resistance of the cell appeared to grow linearly with the test cycle number and time$^{1/2}$ with the test calendar life. Therefore, the resistance increment is defined by:

$$Z_{increment}\left(T, \sqrt{t}, N\right) = k_3(T, N) + k_4(T, \sqrt{t}) \quad (26)$$

In reality, this estimation is simple. The battery increment impedance block consists of only two parameters: k_3 and k_4. The values of the impedances obtained for each characterization test were utilized to obtain the impedance increment dependencies for both aging tests. They are represented in Figs. 12 and 13. Note that the data obtained from the cycle aging tests allowed us to employ a surface-fitting equation to estimate the parameter k_3. A curve fitting was then also employed using MATLAB's curve-fitting tool. The type of fit employed was custom equation:

$$k_3(N) = a + b.\sin(m.T.N.\Omega) + c.exp^{-(w.N)^2} \quad (27)$$

with a = 1.5, b= -0.06, c = -0.498, m = 0.818, and w = 0.82 as the fitting parameters, and N and T are the variables accounting for the cycle number and the temperature, respectively.

Finally, the most reasonable fit to the calendar parameter A was, thus, found to be a 3rd-order polynomial fit given by the expression:

$$k_4(T, \sqrt{t}) = 6.10^{-5}\sqrt{t}^3 - 2.10^{-4}\sqrt{t}^2 - 9.10^{-4}\sqrt{t} + 1 \quad (28)$$

Finally, for a better understanding, a schematic of the overall model is displayed in Fig. 14.

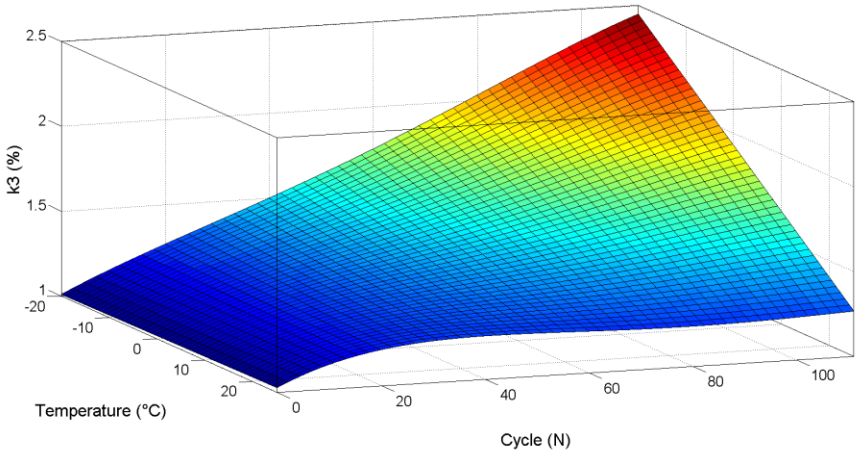

Fig. 12. Tridimensional surface plot of k3 as a function of cycle number and temperature, in case of cell impedance increment produced by cycling.

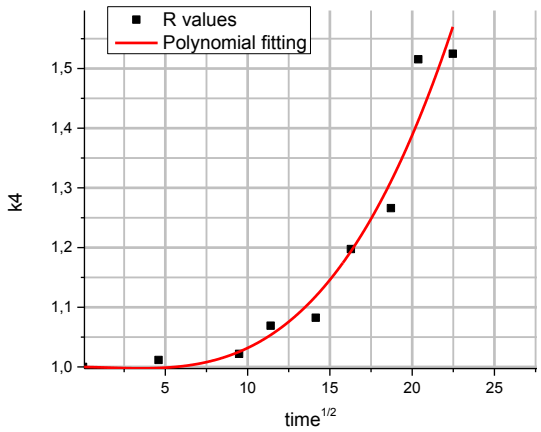

Fig. 13. Three-order polynomial curve of k4 as a function of storage time and temperature, in case of cell impedance variation produced by calendar life.

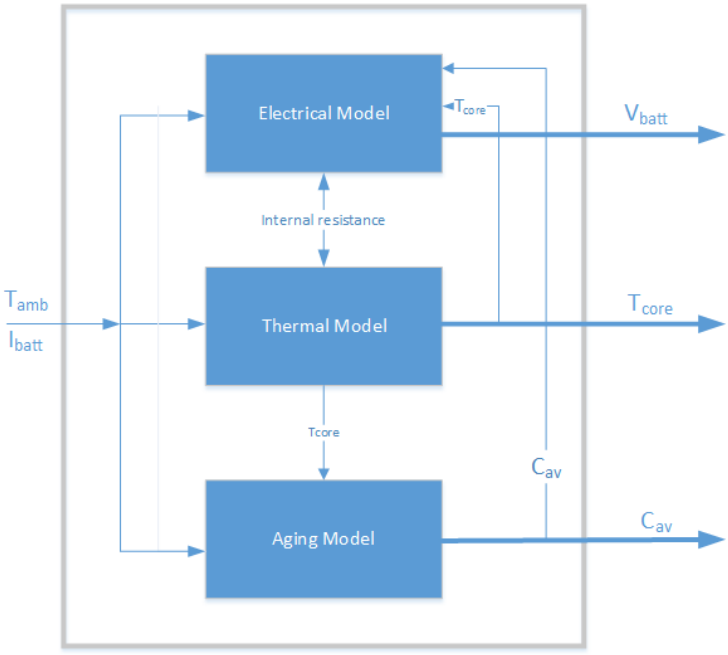

Fig. 14. Overall schematic of the model.

IV. Model Results and Discussions

Once the methodology for predicting future battery lifetime was finalized, it was employed on new sets of battery aging data, and one single cell that has the same characteristics than the previous three battery cells was tested under one temperature of aging: 0°C. The results of this accelerated lifetime test and the simulation associated produced by the lifetime model are shown in this section. Tables V and VI summarizes all results for the experiment, the simulation and error calculation. Different errors were calculated: the error on capacities measurement, the error on the temperature assessment, the mean and maximum values. Given the data of aging tests and simulation values, the approximation error for the capacity fade for all cycle numbers (or storage times) is defined as:

$$\varepsilon_{capa} = \frac{|C_{exp} - C_{sim}|}{0.2C_{exp}} \times 100 \qquad (29)$$

where ε_{capa} is the capacities error (%), C_{exp} is the discharged capacity experimental value (Ah) and C_{sim} is the discharged capacity simulation value (Ah) at a given cycle. The capacities error is actually the error based on the functional lifetime of the cell: 0-20%. Thereby, in the equation 29, a 0.2 coefficient is found at the denominator.

Alternatively, the temperatures error was calculated by:

$$\varepsilon_{temp} = \sum_{i=1}^{N} \frac{\left(\frac{|T_{exp(i)} - T_{sim(i)}|}{T_{exp(i)}}\right)}{N} \times 100 \qquad (30)$$

with i= 1,2,3…N the maximum number of points of a discharge curve, ε_{temp} the temperatures error (%). T_{exp} is the experimental temperature values of all data points (Ah) and T_{sim} is the simulation temperature values of all data points (Ah) for a discharging curve at a given cycle. Given the amount of data points, only the mean value of ε_{temp} is listed.

For each error, the maximum and mean values were determined as follow. As the names suggest, the mean value is an average of the capacities or temperature errors and the maximum is the maximum value found comparing all cycle numbers or storage times, the latter is underlined in **red** in each table. For example, for the capacities error; the mean and maximum values are defined by:

$$\varepsilon_{max} = \max(\varepsilon_{capa}) \quad (31)$$

$$\varepsilon_{mean} = \mathrm{mean}(\varepsilon_{capa}) \quad (32)$$

where ε_{max} is the maximum value (%) and ε_{mean} is the mean value (%).

A. Cycle aging results

In this subsection, a new aging test was performed for validation of the aging model. The results of the simulation and of the experiments are presented here from two angles: the capacity fade and impedance rise. The cell was cycled at a temperature T_{test} of 0°C to continue the investigation of the low temperature's influence on battery aging. The experiment conducted followed the cycling protocol presented in Section II.B.

1) Capacity fade results

Fig. 16 shows the comparison of the capacity fade simulation (represented by the dashed lines) with the measured data for the cycle life test. Capacity fade (Fig. 15) increases rapidly at 0°C, and the end-of-life criterion of 80% of the original capacity under this condition is reached only after 111 cycles. This result indicates the presence of other mechanisms below 25°C, like lithium plating [24], [39]. At each charge cycle, the anode will be plated, and it will consume cyclable Li of both the electrolyte and anode resulting in a rise of the capacity fade [23], [37].

The measured cycling data replicated the simulation results quite well as shown in Fig. 15; the capacities errors values remain indeed below 5% with a maximal error of 4% found at 60 cycles. The data suggest that the cycling data followed a linear function with cycling number. As a result, the simple linear aging model for the cell capacity is able to make estimations of the battery lifetime.

2) Resistance increment results

Fig. 16 shows the simulation results for the resistance increment assessment by plotting the temperature, T_{core},

evolution through cycle aging. The simulation data are represented in dashed lines in Fig. 16. Again, as the cell ages, the internal resistance increases. This result emphasizes an indication of the lithium plating mechanism below 0°C. The growth of the SEI is making a layer impermeable enough that Li^+ ions cannot efficiently pass through the SEI; hence, cell impedance rises [38]. As it can be pointed out from the analysis of the results, the thermal model provides estimation with 8.8% of mean error with a maximal error found for 16 cycles. Such a high value would be alarming but the estimated temperature is only untrue by 1°C, which is acceptable in our application. As a consequence, the good model agreement of the thermal behavior with experimental results also underlines the validation of the model developed in this work.

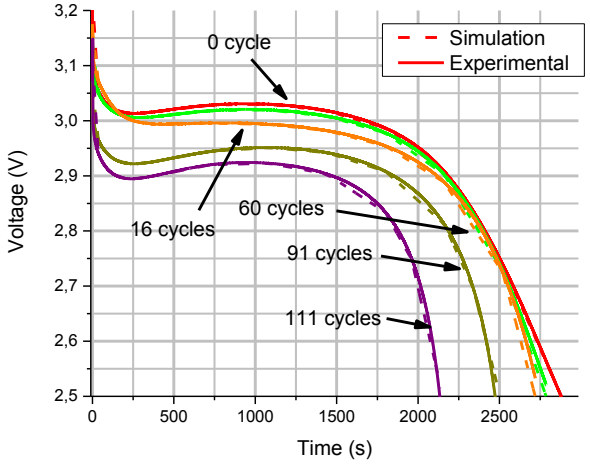

Fig. 15. Evolution of the capacity as the cell ages for cycle aging test at 0°C as well as the simulation results displayed in dashed lines.

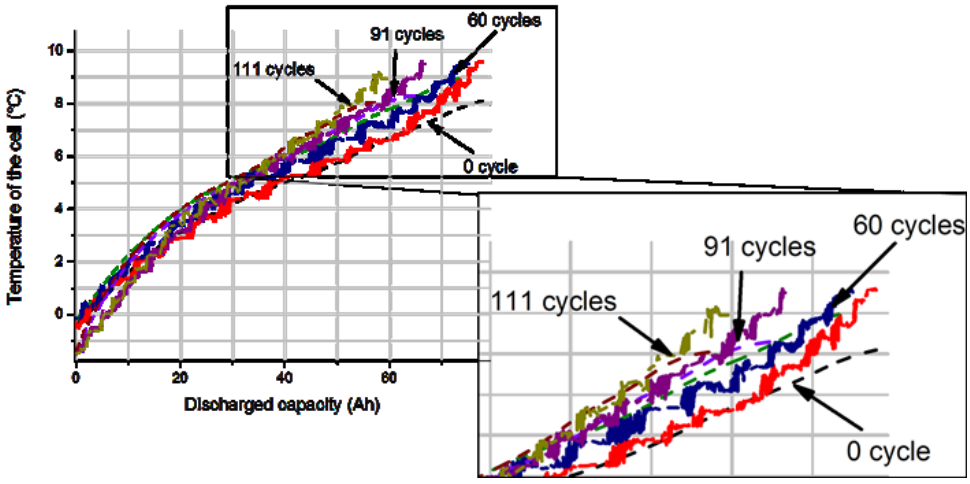

Fig. 16. Evolution of the temperature T_{core} vs discharging capacity for cycle aging test at 0°C as well as the simulation results displayed in dashed lines.

TABLE V. OUTPUT DATA OF THE CYCLE LIFE TEST AT 0°C

T_{test} (°C)	Capacity fade results			
	Testing	***Initial capacity measured (Ah)***	***Final capacity measured (Ah)***	***Number of cycle (or time) before end-of-life criterion (80% of the cell's initial capacity)***
0	Cycling	80.1	63.6	*111 cycles = 555 hours*

T_{test} (°C)	Resistance increment results				
	Testing	***Number of cycle***	***Measured resistance (mΩ)***	***T_{core} initial value (°C)***	***T_{core} maximal value (°C)***
0	Cycling	*0*	2.01	-0.58	8.3
		111 cycles = 555 hours	3.41	-1.5	9.05

	Error calculation				
Ttest (°C)	***Observation***	***Number of cycle***	***Measured value***	***Simulated value***	***Capacities error (%)***
0	Discharged capacity (Ah)	*0*	80.1	80.5	2.5
		16	78.3	77.6	**4.5**
		60	76.2	75.8	2.6
		91	68.1	68.9	3.7
		111	59.4	59.7	2.5
	Mean error (%)				3.2
	T_{core} maximal value (°C)	***Number of cycle***	***Temperatures error of all data points of the curve (%)***		
		0	9		
		60	**12**		
		91	8		
		111	6		
	Mean error (%)		8.8		

B. Calendar aging results

In this subsection, the results of the calendar aging simulation are discussed, likewise, from two points of view: the capacity fade and resistance increment. All the experimental data for calendar lifetime test are already displayed in Table I and II, and the error calculation is summarized in Table V.

1) Capacity fade results

Fig. 17 presents the results of the capacity fade measurement and simulation (in dashed lines) for the calendar aging

test at -20°C. The estimated voltage profiles in Fig. 18 also agree closely with the experimental test. As the plot indicates, the voltage from the simulation matches the actual voltage very closely with a mean temperatures error estimated fewer than 8.8% and the maximum value found at 50 cycles. As a concluding remark, the simple mathematical model describing the calendar lifetime behavior is accurate.

2) Resistance increment results

The result from the temperature T_{core} evolution during aging in Fig. 18 indicates that the temperature of aging is correlated with the change in cell's impedance. A higher heat rejection is found at the end of life of the cell than at the first phase. In addition, despite the high temperatures error percentage (13%) and the mean error (8.5%), the estimated temperature (dashed line in Fig. 18) shows a pretty good trend with the experimental data.

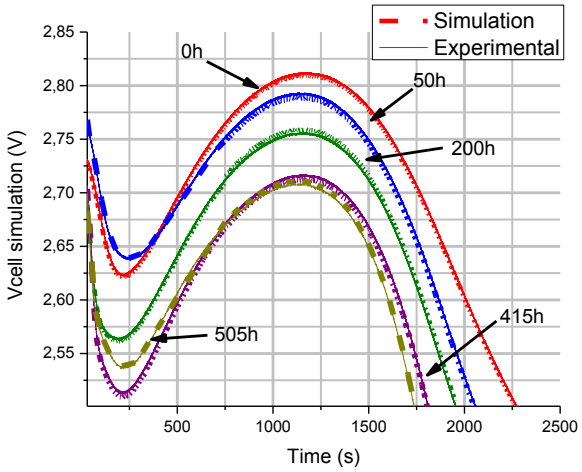

Fig. 17. Evolution of the capacity as the cell ages for calendar lifetime test at -20°C as well as the simulation results displayed in dashed lines.

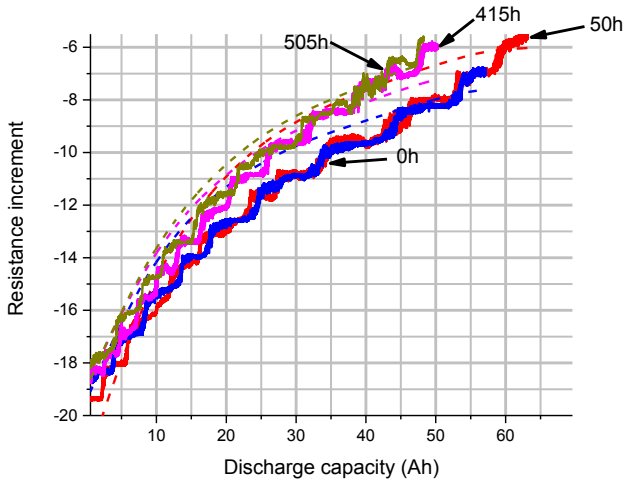

Fig. 18. Evolution of the temperature T_{core} vs discharging capacity for calendar lifetime at -20°C as well as the simulation results displayed in dashed lines.

TABLE VI. ERROR CALCULATION OF THE CALENDAR LIFE TEST AT -20°C

Ttest (°C)	*Observation*	*Number of cycle*	*Measured value*	*Simulated value*	*Capacities error (%)*
-20	Discharged capacity (Ah)	*0*	63.1	63.3	1.6
		50	57.1	57.6	**4.4**
		200	54.2	54.4	1.9
		415	50.3	50.5	1.9
		505	49.3	49.5	2
	Mean error (%)				2.3
	T_{core} maximal value (°C)	***Number of cycle***	***Mean temperatures error of all data points of the curve (%)***		
		0	**13**		
		50	7		
		415	8		
		505	4		
	Mean error (%)		8		

V. CONCLUSION

In this paper, a lifetime analysis at low temperatures based on available experimental data was presented. Lithium-ion cells were aged through severe aging protocols spanning cycle aging and calendar aging. The experimental results show that the capacity loss is strongly affected by low temperatures. For example, the end-of-life criterion was reached only until 12 cycles at -20°C and only 17 days of storage. In addition, a correlation between temperature of the cell and the internal resistance showed a noticeable progressive rise of the impedance as the cell aged especially at low temperatures.

Known aging studies explained this rapid aging rate with the presence of new mechanism in cold weather: the lithium plating. As the results shown, the known degradation consequences of this mechanism are all accelerated: loss of cyclable lithium, loss of electrode active materials, and decrease of accessible surface area (equals an impedance rise).

Alternatively, a lifetime model based on an existing electro-thermal model was developed to reproduce the temperature effect on capacity fade and resistance increment at low temperatures. Data collected during aging tests and simple equations for the aging parameters were used as basis in developing a mathematical aging model.

To obtain reliable validation results, an accelerated cycle test was performed on the cell at 0°C. The data obtained were confronted with simulation results. The result interpretations again point towards a worsening operation of cell

below 0°C but also to good performance of the aging model. The same goes with the calendar aging model; the simple mathematical model is accurate, and the SEI growth represented by the variable k_2 is well reproduced.

Overall, a simple battery life model that accounts for cycle aging and calendar aging at low temperature and that achieves qualitative agreement with experimental data was established.

As a consequence, the resulting aging model can be used to predict both cell's electro-thermal behavior [16] and the remaining capacity at low temperature (from -20°C to 0°C). Future work could focus on developing a battery thermal management system for HEVs for winter applications considering aging mechanisms.

ACKNOWLEDGEMENT

This work is supported by the Natural Sciences and Engineering Research Council of Canada and the Avenir Lyon Saint-Etienne Program (PALSE) of the University of Lyon (FRANCE).

REFERENCES

[1] D. Linden and T. B. Reddy, *HANDBOOK OF BATTERIES 3rd Edition*. McGraw-Hill, 2002.

[2] M. Urbain, M. Hinaje, B. Davat, and P. Desprez, "Energetical Modeling of Lithium-Ion Batteries Including Electrode Porosity Effects," *IEEE Trans. Energy Convers.*, vol. 25, no. 3, pp. 862–872, 2010.

[3] L. Wang, E. G. Collins, S. Member, and H. Li, "Optimal Design and Real-Time Control for Energy Management in Electric Vehicles," *IEEE Trans. Veh. Technol.*, vol. 60, no. 4, pp. 1419–1429, 2011.

[4] A. Lajunen and J. Suomela, "Evaluation of Energy Storage System Requirements for Hybrid Mining Loaders," *IEEE Trans. Veh. Technol.*, vol. 61, no. 8, pp. 3387–3393, Oct. 2012.

[5] D. Doughty and E. P. Roth, "A General Discussion of Li Ion Battery Safety," *Electrochem. Soc. Interface*, vol. 21, no. 2, pp. 37–44, 2012.

[6] R. Klein, N. A. Chaturvedi, J. Christensen, J. Ahmed, R. Findeisen, and A. Kojic, "Optimal charging strategies in lithium-ion battery," *Proc. 2011 Am. Control Conf.*, pp. 382–387, Jun. 2011.

[7] L. Gaines, "Recycling of Li-Ion Batteries," *Argonne Natl. Lab.*, 2011.

[8] O. Veneri, L. Ferraro, C. Capasso, and D. Iannuzzi, "Charging infrastructures for EV: Overview of technologies and issues," *2012 Electr. Syst. Aircraft, Railw. Sh. Propuls.*, pp. 1–6, Oct. 2012.

[9] J. Jaguemont, L. Boulon, Y. Dubé, and D. Poudrier, "Low Temperature Discharge Cycle Tests for a Lithium Ion Cell," *Veh. Power Propuls. Conf.*, pp. 1–6, 2014.

[10] Y. Ji, Y. Zhang, and C.-Y. Wang, "Li-Ion Cell Operation at Low Temperatures," *J. Electrochem. Soc.*, vol. 160, no. 4, pp. A636–A649, Feb. 2013.

[11] N. Omar, P. Van Den Bossche, G. Mulder, M. Daowd, J. M. Timmermans, J. Van Mierlo, and S. Pauwels, "Assessment of Performance of Lithium Iron Phosphate Oxide , Nickel Manganese Cobalt Oxide and Nickel Cobalt Aluminum Oxide Based cells for Using in Plug-in Battery Electric Vehicle Applications," *Veh. Power Propuls. Conf.*, 2011.

[12] S. Bhide and T. Shim, "Novel Predictive Electric Li-Ion Battery Model Incorporating Thermal and Rate Factor Effects," *IEEE Trans. Veh. Technol.*, vol. 60, no. 3, pp. 819–829, 2011.

[13] N. Watrin, R. Roche, H. Ostermann, B. Blunier, A. Miraoui, and S. Member, "Multiphysical Lithium-Based Battery Model for Use in State-of-Charge Determination," *IEEE Trans. Veh. Technol.*, vol. 61, no. 8, pp. 3420–3429, 2012.

[14] O. Erdinc, B. Vural, and M. Uzunoglu, "A dynamic lithium-ion battery model considering the effects of temperature and capacity fading," *2009 Int. Conf. Clean Electr. Power*, pp. 383–386, Jun. 2009.

[15] N. Omar and M. Daowd, "Assessment of performance characteristics of lithium-ion batteries for PHEV vehicles applications based on a newly test methodology," *25th World Batter. Hybrid Fuel Cell Electr. Veh. Symp. Exhib.*, 2010.

[16] J. Jaguemont, L. Boulon, and Y. Dube, "Characterization and modeling of a Hybrid Electric Vehicle Lithium – Ion Battery at Low Temperatures," *IEEE Trans. Veh. Technol.*, no. 99, p. 1, 2015.

[17] Y. Ji and C. Y. Wang, "Heating strategies for Li-ion batteries operated from subzero temperatures," *Electrochim. Acta*, vol. 107, pp. 664–674, Sep. 2013.

[18] H. Songl, J. Jeong, B. Lee, and D. H. Shin, "Experimental Study on the Effects of Pre-Heating a Battery in a Low-Temperature Environment," *Veh. Power Propuls. Conf.*, pp. 1198–1201, 2012.

[19] M. A. Roscher, S. Member, J. Assfalg, and O. S. Bohlen, "Detection of Utilizable Capacity Deterioration in Battery Systems," *IEEE Trans. Veh. Technol.*, vol. 60, no. 1, pp. 98–103, 2011.

[20] J. Wang, P. Liu, J. Hicks-Garner, E. Sherman, S. Soukiazian, M. Verbrugge, H. Tataria, J. Musser, and P. Finamore, "Cycle-life model for graphite-LiFePO4 cells," *J. Power Sources*, vol. 196, no. 8, pp. 3942–3948, Apr. 2011.

[21] M. Uno and K. Tanaka, "Influence of High-Frequency Charge–Discharge Cycling Induced by Cell Voltage Equalizers on the Life Performance of Lithium-Ion Cells," *IEEE Trans. Veh. Technol.*, vol. 60, no. 4, pp. 1505–1515, May 2011.

[22] P. Lu, C. Li, E. W. Schneider, and S. J. Harris, "Chemistry, Impedance, and Morphology Evolution in Solid Electrolyte Interphase Films during Formation in Lithium Ion Batteries," *J. Phys. Chem. C*, vol. 118, no. 2, pp. 896–903, Jan. 2014.

[23] G. Sarre, P. Blanchard, and M. Broussely, "Aging of lithium-ion batteries," *J. Power Sources*, vol. 127, no. 1–2, pp. 65–71, Mar. 2004.

[24] S. Tippmann, D. Walper, L. Balboa, B. Spier, and W. G. Bessler, "Low-temperature charging of lithium-ion cells part I: Electrochemical modeling and experimental investigation of degradation behavior," *J. Power Sources*, vol. 252, pp. 305–316, Apr. 2014.

[25] K. Murashko and J. Pyrh, “Three-Dimensional Thermal Model of a Lithium Ion Battery for Hybrid Mobile Working Machines : Determination of the Model Parameters in a Pouch Cell,” *IEEE Trans. Energy Convers.*, vol. 28, no. 2, pp. 335–343, 2013.

[26] A. Samba, N. Omar, H. Gualous, O. Capron, P. Van den Bossche, and J. Van Mierlo, “Impact of Tab Location on Large Format Lithium-Ion Pouch Cell Based on Fully Coupled Tree-Dimensional Electrochemical-Thermal Modeling,” *Electrochim. Acta*, vol. 147, pp. 319–329, Nov. 2014.

[27] Z. Hilmi, C. H. E. Daud, D. Chrenko, E. Aglzim, A. Keromnes, and L. Le, “Experimental Study of Lithium-ion Battery Thermal Behaviour for Electric and Hybrid Electric Vehicles,” *Veh. Power Propuls. Conf.*, 2014.

[28] J. Kim, S. Member, and B. H. Cho, “State-of-Charge Estimation and State-of-Health Prediction of a Li-Ion Degraded Battery Based on an EKF Combined With a Per-Unit System,” *IEEE Trans. Veh. Technol.*, vol. 60, no. 9, pp. 4249–4260, 2011.

[29] J. D. Dogger, B. Roossien, and F. D. J. Nieuwenhout, “Characterization of Li-Ion Batteries for Intelligent Management of Distributed Grid-Connected Storage,” *IEEE Trans. Energy Convers.*, vol. 26, no. 1, pp. 256–263, 2011.

[30] G. Ning, B. Haran, and B. N. Popov, “Capacity fade study of lithium-ion batteries cycled at high discharge rates,” *J. Power Sources*, vol. 117, no. 1–2, pp. 160–169, May 2003.

[31] T. Kim, S. Member, and W. Qiao, “A Hybrid Battery Model Capable of Capturing Dynamic Circuit Characteristics and Nonlinear Capacity Effects,” *IEEE Trans. Energy Convers.*, vol. 26, no. 4, pp. 1172–1180, 2011.

[32] C. Alaoui, “Solid-State Thermal Management for Lithium-Ion EV Batteries,” *IEEE Trans. Veh. Technol.*, vol. 62, no. 1, pp. 98–107, 2013.

[33] A. Tani, M. B. Camara, and B. Dakyo, “Energy Management Based on Frequency Approach for Hybrid Electric Vehicle Applications : Fuel-Cell/Lithiuml-Battery and Ultracapacitors,” *IEEE Trans. Veh. Technol.*, vol. 61, no. 8, pp. 3375–3386, 2012.

[34] D. V. Do, C. Forgez, K. El, K. Benkara, and G. Friedrich, “Impedance Observer for a Li-Ion Battery Using Kalman Filter,” *IEEE Trans. Veh. Technol.*, vol. 58, no. 8, pp. 3930–3937, 2009.

[35] K. Qian, C. Zhou, V. Yuan, and M. Allanl, “Temperature Effect on Electric Vehicle Battery Cycle Life in Vehicle-to-Grid Applications,” *Electr. Distrib. (CICED), 2010 China Int. Conf. Electr. Distrib.*, pp. 1–6, 2010.

[36] J. Vetter, P. Novák, M. R. Wagner, C. Veit, K.-C. Möller, J. O. Besenhard, M. Winter, M. Wohlfahrt-Mehrens, C. Vogler, and A. Hammouche, “Ageing mechanisms in lithium-ion batteries,” *J. Power Sources*, vol. 147, no. 1–2, pp. 269–281, Sep. 2005.

[37] M. Broussely, P. Biensan, F. Bonhomme, P. Blanchard, S. Herreyre, K. Nechev, and R. J. Staniewicz, “Main aging mechanisms in Li ion batteries,” *J. Power Sources*, vol. 146, no. 1–2, pp. 90–96, Aug. 2005.

[38] D. Aurbach, Y. Talyosef, B. Markovsky, E. Markevich, E. Zinigrad, L. Asraf, J. S. Gnanaraj, and H.-J. Kim, “Design of electrolyte solutions for Li and Li-ion batteries: a review,” *Electrochim. Acta*, vol. 50, no. 2–3, pp. 247–254, Nov. 2004.

[39] T. Waldmann, M. Wilka, M. Kasper, M. Fleischhammer, and M. Wohlfahrt-Mehrens, "Temperature dependent ageing mechanisms in Lithium-ion batteries – A Post-Mortem study," *J. Power Sources*, vol. 262, pp. 129–135, Sep. 2014.

[40] N. Gunawardhana, N. Dimov, M. Sasidharan, G.-J. Park, H. Nakamura, and M. Yoshio, "Suppression of lithium deposition at sub-zero temperatures on graphite by surface modification," *Electrochem. commun.*, vol. 13, no. 10, pp. 1116–1118, Oct. 2011.

[41] K. Tasaki, A. Goldberg, J.-J. Lian, M. Walker, A. Timmons, and S. J. Harris, "Solubility of Lithium Salts Formed on the Lithium-Ion Battery Negative Electrode Surface in Organic Solvents," *J. Electrochem. Soc.*, vol. 156, no. 12, p. A1019, 2009.

[42] J. Belt, V. Utgikar, and I. Bloom, "Calendar and PHEV cycle life aging of high-energy, lithium-ion cells containing blended spinel and layered-oxide cathodes," *J. Power Sources*, vol. 196, no. 23, pp. 10213–10221, Dec. 2011.

[43] S. J. Moura, S. Member, J. C. Forman, S. Bashash, J. L. Stein, and H. K. Fathy, "Optimal Control of Film Growth in Lithium-Ion Battery Packs via Relay Switches," *IEEE Trans. Energy Convers.*, vol. 58, no. 8, pp. 3555–3566, 2011.

[44] B. Y. Liaw, R. G. Jungst, and D. H. Doughty, "Modeling Capacity Fade in Lithium-Ion Cells," *Electrochem. Soc. Inc.*, no. 808, p. 96821, 2003.

[45] U. Tröltzsch, O. Kanoun, and H.-R. Tränkler, "Characterizing aging effects of lithium ion batteries by impedance spectroscopy," *Electrochim. Acta*, vol. 51, no. 8–9, pp. 1664–1672, Jan. 2006.

[46] R. Spotnitz, "Simulation of capacity fade in lithium-ion batteries," *J. Power Sources*, vol. 113, no. 2002, pp. 72–80, 2003.

[47] T. Huria, M. Ceraolo, J. Gazzarri, and R. Jackey, "High Fidelity Electrical Model with Thermal Dependence for Characterization and Simulation of High Power Lithium Battery Cells," *Electr. Veh. Conf. (IEVC), 2012 IEEE Int.*, pp. 1 – 8, 2012.

[48] A. Szumanowski, "Battery Management System Based on Battery Nonlinear Dynamics Modeling," *IEEE Trans. Veh. Technol.*, vol. 57, no. 3, pp. 1425–1432, May 2008.

[49] M. Daowd, N. Omar, B. Verbrugge, P. Van Den Bossche, and J. Van Mierlo, "Battery Models Parameter Estimation based on Matlab / Simulink ®," *25th World Batter. Hybrid Fuel Cell Electr. Veh. Symp. Exhib. Batter.*, vol. 2, pp. 5–9, 2010.

[50] W. M. Haynes, *CRC Handbook of Chemistry and Physics*, 90th ed. 2011.

[51] K. Smith, G.-H. Kim, and A. A. Pesaran, "Modeling of Nonuniform Degradation in Large-Format Li-ion Batteries," *215th Electrochem. Soc. Meet.*, vol. 25, 2009.

[52] I. Bloom, B. W. Cole, J. J. Sohn, S. A. Jones, E. G. Polzin, V. S. Battaglia, and G. L. Henriksen, "An accelerated calendar and cycle life study of Li-ion cells," *J. Power Sources*, vol. 101, no. 2, pp. 238–247, Oct. 2001.

[53] C. Guenther, B. Schott, W. Hennings, P. Waldowski, and M. A. Danzer, "Model-based investigation of electric vehicle battery aging by means of vehicle-to-grid scenario simulations," *J. Power Sources*, vol. 239, pp. 604–610, Oct. 2013.

[54] M. Broussely, S. Herreyre, P. Biensan, P. Kasztejna, K. Nechev, and R. J. Staniewicz, “Aging mechanism in Li ion cells and calendar life predictions,” *J. Power Sources*, vol. 97–98, pp. 13–21, Jul. 2001.

[55] O. Bohlen and J. Kowal, “Ageing behaviour of electrochemical double layer capacitors,” *J. Power Sources*, vol. 173, no. 1, pp. 626–632, Nov. 2007.

[56] Ploehn, H. J, P. Ramadass, and E. W. Ralph, “Solvent Diffusion Model for Aging of Lithium-Ion Battery Cells,” *J. Electrochem. Soc.*, vol. 151, pp. A456–A462, 2004.

[57] N. Omar, M. A. Monem, Y. Firouz, J. Salminen, J. Smekens, O. Hegazy, H. Gaulous, G. Mulder, P. Van den Bossche, T. Coosemans, and J. Van Mierlo, “Lithium iron phosphate based battery – Assessment of the aging parameters and development of cycle life model,” *Appl. Energy*, vol. 113, pp. 1575–1585, Jan. 2014.

[58] Y. Zhang and C.-Y. Wang, “Cycle-Life Characterization of Automotive Lithium-Ion Batteries with LiNiO2 Cathode,” *J. Electrochem. Soc.*, vol. 156, no. 7, p. A527, 2009.